


A new Miocene ape and locomotion in the ancestor of great apes and humans

Article | Published: 06 November 2019

A new Miocene ape and locomotion in the ancestor of great apes and humansMadelaine Böhme , Nikolai Spassov, Jochen Fuss, Adrian Tröscher, Andrew S. Deane, Jérôme Prieto, Uwe Kirscher, Thomas Lechner & David R. Begun*Nature* **575**, 489–493(2019)**13k** Accesses | **11** Citations | **806** Altmetric | [Metrics](#)**Abstract**

Many ideas have been proposed to explain the origin of bipedalism in hominins and suspension in great apes (hominids); however, fossil evidence has been lacking. It has been suggested that bipedalism in hominins evolved from an ancestor that was a palmigrade quadruped (which would have moved similarly to living monkeys), or from a more suspensory quadruped (most similar to extant chimpanzees)¹. Here we describe the fossil ape *Danuvius guggenmosi* (from the Allgäu region of Bavaria) for which complete limb bones are preserved, which provides evidence of a newly identified form of positional behaviour—extended limb clambering. The 11.62-million-year-old *Danuvius* is a great ape that is dentally most similar to *Dryopithecus* and other European late Miocene apes. With a broad thorax, long lumbar spine and extended hips and knees, as in bipeds, and elongated and fully extended forelimbs, as in all apes (hominoids), *Danuvius* combines the adaptations of bipeds and suspensory apes, and provides a model for the common ancestor of great apes and humans.

Access through your institution

[Buy or subscribe](#)

Access options

Get time limited or full article access on ReadCube.

from **\$8.99**

[Rent or Buy](#)

All prices are NET prices.

Get full journal access for 1 year

220,50 €

only 4,32 € per issue

[Subscribe](#)

All prices include VAT for France.

Additional access options:

[Log in](#)

[Access through your institution](#)

[Learn about institutional subscriptions](#)

Data availability

All data generated or analysed during this study are included in this published Article (and its [Supplementary Information](#)). The computed tomography scans are available from the corresponding author on reasonable request. The new taxon has the following Life Science Identifier: <http://zoobank.org/References/E1573024-9543-4B1E-A79B-6E40896A4617>.

References

1. Begun, D. R. in *Biped to Strider: The Emergence of Modern Human Walking* (eds Meldrum, D. J. & Hilton, C. E.) 9–33 (Kluwer, 2004).

2. Begun, D. R. & Kivell, T. L. Knuckle-walking in *Sivapithecus*? The combined effects of homology and homoplasy with possible implications for pongine dispersals. *J. Hum. Evol.* **60**, 158–170 (2011).
3. Richmond, B. G., Begun, D. R. & Strait, D. S. Origin of human bipedalism: the knuckle-walking hypothesis revisited. *Am. J. Phys. Anthropol.* **116**, 70–105 (2001).
4. Crompton, R. H., Sellers, W. I. & Thorpe, S. K. Arboreality, terrestriality and bipedalism. *Phil. Trans. R. Soc. Lond. B* **365**, 3301–3314 (2010).
5. Begun, D. R. Dryopithecins, Darwin, de Bonis, and the European origin of the African apes and human clade. *Geodiversitas* **31**, 789–816 (2009).
6. Begun, D. R., Nargolwalla, M. C. & Kordos, L. European Miocene hominids and the origin of the African ape and human clade. *Evol. Anthropol.* **21**, 10–23 (2012).
7. Alba, D. M. Fossil apes from the vallès-enedès basin. *Evol. Anthropol.* **21**, 254–269 (2012).
8. Langergraber, K. E. et al. Generation times in wild chimpanzees and gorillas suggest earlier divergence times in great ape and human evolution. *Proc. Natl Acad. Sci. USA* **109**, 15716–15721 (2012).
9. Moyà-Solà, S. & Köhler, M. A *Dryopithecus* skeleton and the origins of great-ape locomotion. *Nature* **379**, 156–159 (1996).
10. Moyà-Solà, S., Köhler, M., Alba, D. M., Casanovas-Vilar, I. & Galindo, J. *Pierolapithecus catalaunicus*, a new Middle Miocene great ape from Spain. *Science* **306**, 1339–1344 (2004).
11. Alba, D. M., Almécija, S., Casanovas-Vilar, I., Méndez, J. M. & Moyà-Solà, S. A partial skeleton of the fossil great ape *Hispanopithecus laietanus* from Can Feu and the mosaic evolution of crown-hominoid positional behaviors. *PLoS ONE* **7**, e39617 (2012).
12. Begun, D. R. in *Handbook of Paleoanthropology* (eds Henke, W. & Tattersall, I.) 1261–1332 (Springer, 2015).

13. **13.** Lovejoy, C. O., Suwa, G., Simpson, S. W., Matternes, J. H. & White, T. D. The great divides: *Ardipithecus ramidus* reveals the postcrania of our last common ancestors with African apes. *Science* **326**, 73–106 (2009).
14. **14.** White, T. D., Lovejoy, C. O., Asfaw, B., Carlson, J. P. & Suwa, G. Neither chimpanzee nor human, *Ardipithecus* reveals the surprising ancestry of both. *Proc. Natl Acad. Sci. USA* **112**, 4877–4884 (2015).
- 15.** Kirscher, U. et al. A biochronologic tie-point for the base of the Tortonian stage in European terrestrial settings: magnetostratigraphy of the topmost Upper Freshwater Molasse sediments of the North Alpine Foreland Basin in Bavaria (Germany). *Newsl. Stratigr.* **49**, 445–467 (2016).
- 16.** Williams, S. A. & Russo, G. A. Evolution of the hominoid vertebral column: the long and the short of it. *Evol. Anthropol.* **24**, 15–32 (2015).
- 17.** Latimer, B. & Ward, C. V. in *The Nariokotome Homo erectus Skeleton* (eds Walker, A. & Leakey, R.) 266–293 (Springer, 1993).
- 18.** Williams, S. A., Middleton, E. R., Villamil, C. I. & Shattuck, M. R. Vertebral numbers and human evolution. *Am. J. Phys. Anthropol.* **159**, 19–36 (2016).
- 19.** Haeusler, M., Regula, S. & Thomas, B. Modern or distinct axial bauplan in early hominins? A reply to Williams (2012). *J. Hum. Evol.* **63**, 557–559 (2012).
- 20.** Nakatsukasa, M. & Kunitatsu, Y. *Nacholapithecus* and its importance for understanding hominoid evolution. *Evol. Anthropol.* **18**, 103–119 (2009).
- 21.** Pilbeam, D. The anthropoid postcranial axial skeleton: comments on development, variation, and evolution. *J. Exp. Zool.* **302B**, 241–267 (2004).
- 22.** Ward, C. V., Walker, A., Teaford, M. F. & Odhiambo, I. Partial skeleton of *Proconsul nyanzae* from Mfangano island, Kenya. *Am. J. Phys. Anthropol.* **90**, 77–111 (1993).
- 23.**

- Ward, C. V., Nalley, T. K., Spoor, F., Tafforeau, P. & Alemseged, Z. Thoracic vertebral count and thoracolumbar transition in *Australopithecus afarensis*. *Proc. Natl Acad. Sci. USA* **114**, 6000–6004 (2017).
- 24.** Williams, S. A. Placement of the diaphragmatic vertebra in catarrhines: implications for the evolution of dorsostability in hominoids and bipedalism in hominins. *Am. J. Phys. Anthropol.* **148**, 111–122 (2012).
- 25.** Ward, C. V., Hammond, A. S., Plavcan, J. M. & Begun, D. R. A late Miocene hominid partial pelvis from Hungary. *J. Hum. Evol.* <https://doi.org/10.1016/j.jhevol.2019.102645> (2019).
- 26.** McCollum, M. A., Rosenman, B. A., Suwa, G., Meindl, R. S. & Lovejoy, C. O. The vertebral formula of the last common ancestor of African apes and humans. *J. Exp. Zool.* **314B**, 123–134 (2010).
- 27.** Lovejoy, C. O. & McCollum, M. A. Spinopelvic pathways to bipedality: why no hominids ever relied on a bent-hip–bent-knee gait. *Phil. Trans. R. Soc. Lond. B* **365**, 3289–3299 (2010).
- 28.** Landis, E. K. & Karnick, P. A three-dimensional analysis of the geometry and curvature of the proximal tibial articular surface of hominoids. In *Proc. SPIE 60560 Three-Dimensional Image Capture and Applications VII 60560K* (International Society for Optics and Photonics, 2006).
- 29.** Frelat, M. A. et al. Evolution of the hominin knee and ankle. *J. Hum. Evol.* **108**, 147–160 (2017).
- 30.** Tardieu, C. Ontogeny and phylogeny of femoro-tibial characters in humans and hominid fossils: functional influence and genetic determinism. *Am. J. Phys. Anthropol.* **110**, 365–377 (1999).
- 31.** DeSilva, J. M. Functional morphology of the ankle and the likelihood of climbing in early hominins. *Proc. Natl Acad. Sci. USA* **106**, 6567–6572 (2009).
- 32.** DeSilva, J. M., Morgan, M. E., Barry, J. C. & Pilbeam, D. A hominoid distal tibia from the Miocene of Pakistan. *J. Hum. Evol.* **58**, 147–154 (2010).

- 33.** Latimer, B., Ohman, J. C. & Lovejoy, C. O. Talocrural joint in African hominoids: implications for *Australopithecus afarensis*. *Am. J. Phys. Anthropol.* **74**, 155–175 (1987).
34. **34.** Thorpe, S. K., Holder, R. L. & Crompton, R. H. Origin of human bipedalism as an adaptation for locomotion on flexible branches. *Science* **316**, 1328–1331 (2007).
- 35.** Thorpe, S. K., McClymont, J. M. & Crompton, R. H. The arboreal origins of human bipedalism. *Antiquity* **88**, 906–914 (2014).
- 36.** Wolpoff, M. *Australopithecus*: a new look at an old ancestor (part 2). *Gen. Anthropol.* **3**, 1–5 (1997).
- 37.** Straus, W. in *Classification and Human Evolution* (ed. Washburn, S. L.) 146–177 (Aldine, 1963).
- 38.** Asfaw, B. et al. *Australopithecus garhi*: a new species of early hominid from Ethiopia. *Science* **284**, 629–635 (1999).
- 39.** Ruff, C. B. Long bone articular and diaphyseal structure in Old World monkeys and apes. II: estimation of body mass. *Am. J. Phys. Anthropol.* **120**, 16–37 (2003).
- 40.** Haile-Selassie, Y. et al. An early *Australopithecus afarensis* postcranium from Woranso-Mille, Ethiopia. *Proc. Natl Acad. Sci. USA* **107**, 12121–12126 (2010).
- 41.** DeSilva, J. M. *Vertical Climbing Adaptations in the Anthropoid Ankle and Midfoot: Implications for Locomotion in Miocene Catarrhines and Plio-Pleistocene Hominins*. PhD thesis, Univ. Michigan, (2008).
- 42.** Behrensmeyer, A. K. The taphonomy and paleoecology of Plio-Pleistocene vertebrate assemblages east of Lake Rudolf, Kenya. *Bull. Mus. Comp. Zool.* **146**, 473–578 (1975).
- 43.** Almécija, S. et al. The femur of *Orrorin tugenensis* exhibits morphometric affinities with both Miocene apes and later hominins. *Nat. Commun.* **4**, 2888 (2013).
- 44.**

- Smith, B. H. Patterns of molar wear in hunger-gatherers and agriculturalists. *Am. J. Phys. Anthropol.* **63**, 39–56 (1984).
- 45.** Smith, T. M., Olejniczak, A. J., Martin, L. B. & Reid, D. J. Variation in hominoid molar enamel thickness. *J. Hum. Evol.* **48**, 575–592 (2005).
- 46.** Martin, L. B. *The Relationships of the later Miocene Hominoidea*. PhD thesis, Univ. College London (1983).
- 47.** Wessel, P. et al. Generic mapping tools: improved version released. *EOS* **94**, 409–410 (2013).
- 48.** Amante, C. & Eakins, B. W. *ETOPO1 1 Arc-Minute Global Relief Model: Procedures, Data Sources and Analysis NOAA Technical Memorandum NESDIS NGDC-24* <https://www.ngdc.noaa.gov/mgg/global/relief/ETOPO1/docs/ETOPO1.pdf> (National Geophysical Data Center, NOAA, 2009).
- 49.** Reuter H. I., Nelson, A. & Jarvis, A. An evaluation of void-filling interpolation methods for SRTM data. *Int. J. Geogr. Inf. Sci.* **21**, 983–1008 (2007).
- 50.** Almécija, S., Alba, D. M. & Moyà-Solà, S. *Pierolapithecus* and the functional morphology of Miocene ape hand phalanges: paleobiological and evolutionary implications. *J. Hum. Evol.* **57**, 284–297 (2009).

Acknowledgements

We are indebted to the following researchers and curators for granting access to collections under their care: S. Moyà-Solà and D. Alba, E. Gilissen, L. Costeur, A. van Heteren, S. Merker, E. Weber. We thank C. Schulbert and J.-F. Metayer for computed tomography scanning, and A. Fatz, H. Stöhr and W. Gerber for technical support.

Author information

Affiliations

1. Department of Geosciences, Eberhard-Karls-Universität Tübingen, Tübingen, Germany

Madeline Böhme, Jochen Fuss, Uwe Kirscher & Thomas Lechner

2. Senckenberg Centre for Human Evolution and Palaeoenvironment, Tübingen, Germany

Madeline Böhme, Jochen Fuss, Adrian Tröscher & Thomas Lechner

3. National Museum of Natural History, Bulgarian Academy of Sciences, Sofia, Bulgaria

Nikolai Spassov

4. Anatomy & Cell Biology, University of Indianapolis, Indianapolis, IN, USA

Andrew S. Deane

5. Paleontology & Geobiology, Ludwig-Maximilians-Universität, Munich, Germany

Jérôme Prieto

6. Earth Dynamics Research Group, School of Earth and Planetary Sciences, Curtin University, Perth, Western Australia, Australia

Uwe Kirscher

7. Department of Anthropology, University of Toronto, Toronto, Ontario, Canada

David R. Begun

Contributions

M.B. and D.R.B. designed the study; M.B., N.S., J.F., A.T., A.S.D., J.P., U.K., T.L. and D.R.B. collected the data and performed the analyses; M.B., D.R.B. and N.S. discussed the results and wrote the paper.

Corresponding author

Correspondence to [Madelaine Böhme](#).

Ethics declarations

Competing interests

The authors declare no competing interests.

Additional information

Publisher's note Springer Nature remains neutral with regard to jurisdictional claims in published maps and institutional affiliations.

Peer review information *Nature* thanks Jeremy M. DeSilva, Tracy Kivell and Salvador Moyà-Solà for their contribution to the peer review of this work.

Extended data figures and tables

Extended Data Fig. 1 Localization of Hammerschmiede locality and excavation plan with localized *D. guggenmosi* specimens.

a, Topographical map of Europe. **b**, Magnification of the western part of the south German Molasse Basin (North Alpine Foreland Basin). The Hammerschmiede locality (47° 55' 37" N, 10° 35.5' E) is highlighted with a black star. Both maps were created using Generic Mapping Tools⁴⁷ and topographic datasets ETOPO1⁴⁸ and SRTM3⁴⁹. **c**, Excavation plan of the HAM 5 layer (the section has previously been published¹⁵) with excavated areas coloured in grey. Intermediate regions represent material lost due to clay mining. Dashed lines indicate the reconstructed thalweg course of the palaeochannel. Different colours and symbols indicate the individual context: holotype (GPIT/MA/10000) adult male marked in red (stars), paratype (GPIT/MA/10001) female 1 in blue (diamonds), paratype (GPIT/MA/10002) juvenile individual in yellow (circles) and paratype (GPIT/MA/10003) female 2 in green (triangles). The red encircled sector indicates removed and

stored sediments that were screen washed separately. This area was under threat of destruction from quarry activity. To avoid the complete loss of this sediment, approximately 25 tonnes were removed for remote processing. Two specimens were recovered in situ in this area. Five other specimens from this area were recovered during subsequent screen washing and cannot be more precisely localized. Coordinates correspond to Gauss-Krüger Zone 4 grid with easting (R) and northing (H) in metres.

Extended Data Fig. 2 *D. guggenmosi*, dental and cranial specimens.

a, Left maxilla with P³–M² (GPIT MA/10000-01) in lateral, anterior, medial (top), palatal, posterior, superior (bottom) views. **b**, Left mandible (GPIT MA/10000-02) in lateral, anterior, medial and occlusal views. **c**, Left upper central incisor (GPIT MA/10002-01) in labial, lingual and occlusal views. **d**, Right upper P³ fragment (GPIT MA/10000-05) in buccal, occlusal and mesial views. **e**, Left P³ (GPIT MA/10001-03) in buccal, occlusal and mesial views. **f**, Right upper M¹ (GPIT MA/10001-01) in occlusal, medial, distal and buccal views. **g**, Left lower P₃ (GPIT MA/10000-07) in medial, buccal, lingual and occlusal views. **h**, Left lower lateral incisor (GPIT MA/10003-5) in distal, mesial, lingual and labial views. **i**, Left lower central incisor (GPIT MA/10000-08) in distal, mesial and lingual views. **j**, Right lower P₃ (GPIT MA/10000-06) in mesial, distal, buccal and occlusal views. **k**, Right lower M₂ (GPIT MA/10000-03) in lingual, buccal (top), mesial, distal (bottom) and occlusal views. **l**, Right lower M₃ (GIPT MA/10000-04) in lingual, mesial (top), buccal, distal (bottom) and occlusal views. Scale bar, 10 mm.

Extended Data Fig. 3 Long-bone relationships and tibial plateau surface area.

a, Relationships of physiologic lengths of tibia and ulna among extant and fossil catarrhines. **b**, Relationships of tibial plateau surface area (TPSA sensu³⁹, natural logarithm of square root) and tibial total length (natural logarithm) among extant hominids, hylobatids and cercopithecids (comparative data from a previous study³⁹). The tibial plateau surface area of GPIT MA/10000-10 is 1,457 mm².

Extended Data Fig. 4 *D. guggenmosi*, additional views of right ulna (GPIT MA/10000-10) and left tibia (GPIT MA/10000-15).

a–d, Lateral (**a**), anteromedial (**b**) and posterior (**c**) views of the ulna and the reconstructed olecranon in anterior view (**d**). **e, f**, Medial (**e**) and lateral (**f**) views of the tibia. Scale bar, 20 mm.

Extended Data Fig. 5 Ulnar trochlear notch, phalangeal, metacarpal and tibial midshaft comparisons.

a, Ulnar trochlear notch angle (for raw data, see Supplementary Table 9). **b**, Hallucal proximal phalanx (PP1) torsion (for measurement, see [Methods](#); for raw data, see Supplementary Table 23). **c**, Size-adjusted hallucal proximal phalanx (PP1) midshaft robusticity ($MLms \times DPms/GM$ in which $MLms$ is the mediolateral width at midshaft, $DPms$ is the dorsopalmar height at midshaft and GM is the geometric mean of the seven measurements: ML and DP at proximal, distal and midshaft, and total length; for raw data, see Supplementary Table 22). **d**, Size-adjusted second manual proximal phalanx (PP2) gracility (TL/GM in which TL is the total length and GM is the geometric mean of five measurements: ML and DP at distal and midshaft, and TL ; five measurements are used to include *Pierolapithecus catalaunicus*, in which the proximal articulation is damaged⁵⁰; for raw data, see Supplementary Table 11). **e**, Manual phalangeal base, ratio of mediolateral (ML) to dorsopalmar (DP) length (for raw data, see Supplementary Tables 11, 12). **f**, Manual metacarpal 1 base, ratio of dorsopalmar to radioulnar (RU) length (for raw data, see Supplementary Table 10). **g**, Relative size of manual metacarpal 1 base (geometric mean of dorsopalmar and radioulnar lengths) to proximal phalanx of ray 2 (geometric mean of seven measurements; for raw data, see Supplementary Tables 10, 11). **h**, Tibial cross-section at midshaft (ratio of anteroposterior and mediolateral width; for raw data see Supplementary Table 21). Sample sizes (n) of biologically independent animals are reported in parentheses below each box plot. All box plots show the centre line (median), box limits (upper and lower quartiles), crosses (arithmetic mean), whiskers (range) and individual values (circles).

Extended Data Fig. 6 Curvature manual proximal phalanges.

Box plots of the first polynomial coefficient (A) of the second-order polynomial functional representing phalangeal shaft curvature. The box represents the interquartile range, which represents 50% of the sample values. The whiskers are lines that extend from the interquartile range box to the highest and lowest values, excluding outliers. The line across the box indicates the median sample value for coefficient A . Extant primates are colour-coded according to locomotor adaptation. Taxa are arranged according to ascending median phalangeal shaft curvature. Sample sizes (n) of biologically independent animals are reported in parentheses after the species names.

Extended Data Fig. 7 *D. guggenmosi*, patella and femora.

a, Right patella (GPIT MA/10000-12) in external and internal views. **b**, Right femur head (GPIT MA/10000-11) in medial, anterior, posterior (top), superior and lateral (bottom) views. **c**, Left femur head (GPIT MA/10001-02) in medial, posterior, anterior (top), superior and lateral (bottom) views. **d**, Left femur, proximal half (GPIT MA/10003-01) in anterior (top) and posterior (bottom) views. Scale bar, 10 mm.

Extended Data Fig. 8 Ellipse estimates of lateral tibial condyle.

Best fit ellipses to digitalized portions of sagittal cross-sections through lateral tibial condyle of *D. guggenmosi* and extant catarrhines. Digitalized dots are shown in colour and best-fit ellipses in black. Orientation of ellipses follows the lateral condyle orientation (dorsal is up, anterior is left) at the same scale (scale bar, 20 mm). Inset shows calculated values of eccentricity for the obtained ellipses. Results indicate that both *Danuvius* and extant humans have a flat lateral tibial condyle (eccentricity >0.85), whereas great apes exhibit a convex lateral condyle (eccentricity <0.80) and *Cercopithecus* occupy an intermediate position.

Extended Data Fig. 9 Hallux length and robusticity.

a, Ratio (natural logarithm) of proximal hallucal phalanx total length to tibial physiologic length, relative to body mass (maximum femur head diameter). **b**, Box plots of hallux to femur head diameter ratios (natural logarithm). Box plots show the centre line (median), box limits (upper and lower quartiles), cross (arithmetic mean), whiskers (range) and individual values (circles). **c**, Size-adjusted hallucal phalanx midshaft robusticity (for explanation, see Extended Data Fig. 8c), relative to femur head diameter. All sample sizes (n) of biologically independent animals are reported in parentheses after the species names. For raw data, see Supplementary Tables 7, 22.

Extended Data Fig. 10 *D. guggenmosi*, maxillary sinus and enamel thickness.

a, Left maxilla with three-dimensional rendering of molar roots and maxillary sinus (blue) in lingual (left), anterior (middle) and occlusal (right) views. Sinus runs deep between the posterobuccal and lingual roots of M^2 , rising anteriorly (dashed black line). Laterally the sinus extends deep into the zygomatic root (dashed white line). **b**, **c**, Enamel thickness measured on right M_2 (GPIT/MA 10000-03). Computed tomography image of the cross-section at distal sectional plane (**b**) and graphical conversion (**c**; grey, enamel; dark grey; dentine).

Supplementary information

Supplementary Information

This file contains Supplementary Sections 1-5 and Supplementary Tables 1-24 – see contents pages for full details.

Reporting Summary

Rights and permissions

[Reprints and Permissions](#)

About this article

Cite this article

Böhme, M., Spassov, N., Fuss, J. *et al.* A new Miocene ape and locomotion in the ancestor of great apes and humans. *Nature* **575**, 489–493 (2019). <https://doi.org/10.1038/s41586-019-1731-0>

Received 10 July 2019 **Accepted** 27 September 2019 **Published** 06 November 2019

Issue Date 21 November 2019 **DOI** <https://doi.org/10.1038/s41586-019-1731-0>

Subjects [Biological anthropology](#) • [Palaeontology](#)

Further reading

- [Revolutionary Fossils, Ancient Biomolecules, and Reflections in Ethics and Decolonization: Paleoanthropology in 2019](#)

Lauren Schroeder

American Anthropologist (2020)

- [Orrorin tugenensis et les origines de l'homme : une synthèse](#)

B. Senut

Bulletin de l'Académie Nationale de Médecine (2020)

- [The large-sized darter *Anhinga pannonica* \(Aves, Anhingidae\) from the late Miocene hominid Hammerschmiede locality in Southern Germany](#)

Gerald Mayr, Thomas Lechner[...], Madelaine Böhme & Jun Liu

PLOS ONE (2020)

- **The evolution of the vestibular apparatus in apes and humans**

Alessandro Urciuoli, Clément Zanolli, Amélie Beaudet, Jean Dumoncel, Frédéric Santos[...], Salvador Moyà-Solà & David M Alba

eLife (2020)

- **A new dryopithecine mandibular fragment from the middle Miocene of Abocador de Can Mata and the taxonomic status of ‘Sivapithecus’ occidentalis from Can Vila (Vallès-Penedès Basin, NE Iberian Peninsula)**

David M. Alba, Josep Fortuny, Josep M. Robles, Federico Bernardini, Miriam Pérez de los Ríos, Claudio Tuniz[...], Salvador Moyà-Solà & Clément Zanolli

Journal of Human Evolution (2020)

Nature

© 2020 Springer Nature Limited